Multigrid Methods for Isogeometric Thin Plate Discretizations

J. Benzaken, C. Coley, J. A. Evans

1 Abstract

In this paper, we present a novel isogeometric approach to the numerical solution of the classical Reissner-Mindlin and Kirchhoff-Love plate equations. This approach eliminates the common issue of locking in thin plates, a numerical phenomenon resulting from an incompatibility between the finite element spaces for the translational and rotational displacement degrees of freedom. This locking-free implementation also permits the use of a simple geometric multigrid method for solving the resulting linear system in which Schwarz methods with intelligently-chosen subdomains are used for iterative smoothing in the multigrid V-cycles. In the thin plate limit, our multigrid approach automatically and exactly preserves the constraint that the shear strain is zero at every geometric level. This results in a method with convergence rates independent of the thickness. Moreover, this elucidates the problem as a network of coupled plates with Dirichlet boundary data specified by adjacent subdomains. Numerical results for both the Kirchhoff-Love and Reissner-Mindlin plates are presented. The results demonstrate the robustness of the numerical method through the invariance of convergence rates with respect to thickness.

2 Introduction - Motivations

Load-bearing structures in a plane-stress state are often modeled through the use of plates and shells. This modeling approach is desirable in comparison to a full three-dimensional elastic model since through-thickness effects can generally be neglected, consequently reducing computational expense. However, there are difficulties associated with their numerical solution. The simplest plate and shell models are based on Kirchhoff-Love theory and were studied largely in the 50's. Due to the 4^{th}-order nature of the governing biharmonic form, C^1 elements are required for compatibility with the weak $\mathcal{H}^2$ solution. The 21 degree-of-freedom Argyris element is a suitable choice for such a model, requiring global continuity at nodes and along edges, as well as continuous nodal first and second derivative data. Unfortunately, the resulting linear system is sorely ill-conditioned. The difficulties associated with constructing well-conditioned and conforming Kirchhoff-Love elements paved the way for the Reissner-Mindlin plate model, a 2^{nd}-order system requiring only requiring C^0 finite elements for its weak $\mathcal{H}^1$ solution. This is accomplished by relating the translational and rotational displacements through an additional shear strain term. Although Reissner-Mindlin plate elements greatly simplify implementation, they suffer from a numerical artifact known as "locking." This phenomenon occurs as thickness vanishes due to the necessity of satisfying a constraint that the shear strain be zero, resulting in an indefinite linear system. For most plate elements, this constraint is much too strong, resulting in a loss of approximability. A solution to this simulation hurdle is to introduce the shear strain as an additional variable and weaken the constraint enforcement by decreasing its order [1]. Unfortunately, linear systems associated with the Reissner-Mindlin plate model typically do not lend themselves to efficient iterative solution procedures due to the locking phenomenon and the indefinite nature of the system as thickness vanishes.

Isogeometric analysis is a novel computational approach which unifies computer-aided design and finite element analysis [4]. Isogeometric analysis has been shown to be a particularly powerful analysis technology for structural mechanics. The arbitrary continuity between elements provided through the isogeometric paradigm permits a trivial implementation of the Kirchhoff-Love plate model, since global C^1 elements are readily available. Additionally, isogeometric discrete differential forms allow for a locking-free implementation of the Reissner-Mindlin plate which satisfy the shear constraint pointwise in the zero-thickness limit, without losing approximability [2]. This further enables the use of multigrid solvers for both Kirchhoff-Love and Reissner-Mindlin plates. This is accomplished through the use of Schwarz iterative methods, a generalization of the Jacobi and Gauss-Seidel smoothers. Rather than smoothing and updating the solution in a node-by-node fashion, we instead define a set of overlapping subdomains [7] on which the Reissner-Mindlin and Kirchhoff-Love plate problems are solved. In the classical setting, these subdomains lock, but the new method introduced is locking-free for any mesh size. This results in a robust and efficient linear solver technology.

3 Isogeometric Analysis

Isogeometric analysis is a modification to the finite element method where rather than using the Lagrange polynomials for performing analysis, we instead use *Non-Uniform Rational B-Splines*, or NURBS. The primary motivation behind this modeling paradigm is to eliminate the design-through-analysis bottleneck - the high expense of creating analysis-suitable meshes from CAD geometries. A tremendous benefit of using the NURBS basis is that the resulting mesh is arbitrarily continuous, in contrast to the typical C^0 finite element counterpart.

The NURBS functions are derived from the B-spline basis. The B-spline basis used for analysis is constructed by first specifying an open knot-vector $\Xi = (\xi_0, \xi_1, \ldots, \xi_{n+p+1})$, a vector of knots ξ_k such that the first and last knot are repeated $p+1$ times. This knot vector describes the *parametric domain* $\hat{\Omega}$ in which the analysis basis exists. Thereafter, the B-splines can be generated through the Cox-deBoor formula given by

$$N_{i,p}(\xi) = \frac{\xi - \xi_i}{\xi_{i+p} - \xi_i} N_{i,p-1}(\xi) + \frac{\xi_{i+p+1} - \xi}{\xi_{i+p+1} - \xi_{i+1}} N_{i+1,p-1}(\xi), \qquad N_{i,0}(\xi) = \begin{cases} 1, & \xi_i \leq \xi < \xi_{i+1} \\ 0, & \text{elsewhere} \end{cases}$$

This formula generates the B-spline basis in one-dimension. The corresponding d-dimensional B-spline basis is obtained through a tensor product of one-dimensional basis functions.

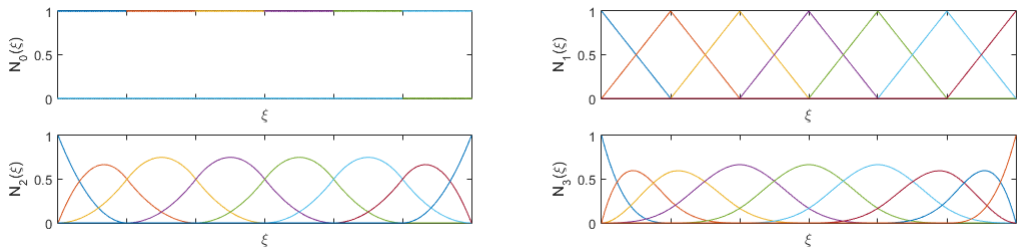

Figure 1: Sets of B-spline basis functions with varying polynomial degrees: constant, linear, quadratic, and cubic.

For more information regarding isogeometric analysis and NURBS basis functions, the reader is referred to [4] and [8].

4 Plate Geometry and Mechanics

In the plate setting, the displacement field is handled in an idealized fashion. The 3-dimensional plate is modeled as a 2-dimensional, planar surface, known as the "midsurface," and through-thickness effects are linearized about this midsurface. The plate is assumed to live in a Euclidean space, though the choice of basis is not necessarily Cartesian. We assume the shell midsurface is defined by an isogeometric representation

$$\mathbf{X}(\boldsymbol{\xi}) = \sum_i \mathbf{P}_i N_{i,p}(\boldsymbol{\xi})$$

where $\{N_{i,p}\}$ are NURBS basis functions and $\{\mathbf{P}_i\}$ are control points. Moreover, the in-plane covariant vectors used in the analysis coordinate frame are defined by the derivative of this mapping with respect to the parametric coordinates,

$$\mathbf{a}_\alpha = \frac{\partial \mathbf{X}}{\partial \xi^\alpha}$$

for $\alpha = 1, 2$. Through these basis vectors, the covariant metric tensor is given by their contraction $\mathrm{a}_{\alpha\beta} = \mathbf{a}_\alpha \cdot \mathbf{a}_\beta$. The contravariant counterpart to the metric tensor is given by the inverse of the covariant metric tensor, $a^{\alpha\beta} = [a_{\alpha\beta}]^{-1}$. Note that throughout this paper, Einstein notation is used, therefore repeated high and low indices invoke a summation between those components.

In what follows, Latin indices correspond to $1, 2, 3$ and Greek indices correspond to $1, 2$. The normal basis vector, used for tracking out-of-plane displacements, is given by

$$\mathbf{a}_3 = \frac{\mathbf{a}_1 \times \mathbf{a}_2}{\|\mathbf{a}_1 \times \mathbf{a}_2\|}$$

The purpose of the metric tensor is used for "raising" and "lowering" indices or equivalently converting vector entities between their covariant (low index) and contravariant (high index) forms. Particularly,

$$u_\alpha = a_{\alpha\beta}u^\beta \quad \text{and} \quad u^\alpha = a^{\alpha\beta}u_\beta$$

Moreover, the contravariant basis is defined as

$$\mathbf{a}^\alpha = a^{\alpha\beta}\mathbf{a}_\beta$$

An arbitrary vector in this frame is represented as

$$\mathbf{u} = u_\alpha \mathbf{a}^\alpha + u_3 \mathbf{a}_3$$

since $\mathbf{a}_3 = \mathbf{a}^3$. With the previous notation established, the displacement of a plate is written as:

$$\mathbf{U}(\xi^1, \xi^2, \xi^3) = \mathbf{u}(\xi^1, \xi^2) + \xi^3 \boldsymbol{\theta}(\xi^1, \xi^2) \tag{1}$$

where the term $\mathbf{u} = u_i \mathbf{a}^i$ represents the translational displacement of the midsurface while the term $\boldsymbol{\theta} = \theta_\alpha \mathbf{a}^\alpha$ represents the rotational displacement of the midsurface. The strong form of the PDE governing the displacement of the plate is given by the internal and external force balance namely,

$$\sigma_{ij,j} = F_i \tag{2}$$

where, in the plate setting, the stress tensor is given by

$$\boldsymbol{\sigma} = \sigma_{ij}\ \mathbf{a}^i \otimes \mathbf{a}^j = \sigma^{ij}\ \mathbf{a}_i \otimes \mathbf{a}_j$$

Under the Hooke's Law assumption, we can express the stress tensor as the contraction of the strain tensor with the stiffness tensor $\hat{C}$,

$$\sigma^{ij} = \hat{C}^{ijkl}\varepsilon_{kl}$$

However, we can further decompose this relationship into its in-plane and out-of-plane components as

$$\sigma^{\alpha\beta} = C^{\alpha\beta\lambda\mu}\varepsilon_{\lambda\mu} \quad \text{and} \quad \sigma^{\alpha 3} = \sigma^{3\alpha} = \frac{1}{2}D^{\alpha\lambda}\varepsilon_{\lambda 3}$$

where the stiffness tensors are given by

$$C^{\alpha\beta\lambda\mu} = \frac{E}{2(1+\nu)}(a^{\alpha\lambda}a^{\beta\mu} + a^{\alpha\mu}a^{\beta\lambda} + \frac{2\nu}{1-\nu}a^{\alpha\beta}a^{\lambda\mu}) \quad \text{and} \quad D^{\alpha\lambda} = \frac{2E}{1+\nu}a^{\alpha\lambda}$$

Now the components of the strain tensor, $\boldsymbol{\varepsilon} = \varepsilon_{ij}\ \mathbf{a}^i \otimes \mathbf{a}^j$, are given by the components of the symmetric part of the gradient of the displacement field therefore,

$$\varepsilon_{ij} = \frac{1}{2}\left(\mathbf{U}_{,i} \cdot \mathbf{a}_j + \mathbf{U}_{,j} \cdot \mathbf{a}_i\right) \tag{3}$$

Note that differentiation of a vector, $\mathbf{v} = v_i \mathbf{a}^i$, with respect to the parametric variable ξ^α in the $\mathbf{a}$-frame is defined as

$$\mathbf{v}_{,\beta} = \frac{\partial}{\partial \xi^\beta}\left(v_\alpha \mathbf{a}^\alpha + v_3 \mathbf{a}_3\right) = v_{\alpha|\beta}\mathbf{a}^\alpha + v_{3,\beta}\mathbf{a}_3$$

where the covariant derivatives of in-plane components are given by

$$u_{\alpha|\beta} = u_{\alpha,\beta} + \Gamma^\lambda_{\alpha\beta}u_\lambda$$

and the *Surface Christoffel Symbols* are defined as

$$\Gamma^\lambda_{\beta\alpha} = \mathbf{a}^\lambda \cdot \mathbf{a}_{\beta,\alpha}$$

Now, after substituting (1) in (3) and simplifiying, we have

$$\begin{aligned} \varepsilon_{\alpha\beta} &= \gamma_{\alpha\beta}(\mathbf{u}) + \xi^3 \chi_{\alpha\beta}(\boldsymbol{\theta}) \\ \varepsilon_{\alpha 3} &= \zeta_\alpha(u_3, \boldsymbol{\theta}) \\ \varepsilon_{33} &= 0 \end{aligned}$$

where

$$\begin{aligned} \gamma_{\alpha\beta}(\mathbf{u}) &= {}^1\!/_2(u_{\alpha|\beta} + u_{\beta|\alpha}) \\ \chi_{\alpha\beta}(\boldsymbol{\theta}) &= {}^1\!/_2(\theta_{\alpha|\beta} + \theta_{\beta|\alpha}) \\ \zeta_\alpha(u_3, \boldsymbol{\theta}) &= {}^1\!/_2(\theta_\alpha + u_{3,\alpha}) \end{aligned} \tag{4}$$

are referred to as the *membrane strain*, *bending strain*, and *shear strain* tensors, respectively. Moreover, in the plate setting we are primarily concerned with transverse displacements. Therefore, we will define $u_3 = w$ (and $v_3 = v$ for virtual displacements) in what follows to clarify subsequent derivations. Refer to [3] for a more detailed derivation and description of the Kirchhoff-Love and Reissner-Mindlin plate models.

5 Isogeometric Thin Plate Discretizations

Up to this point, we have assumed a plate-like displacement field, but we have not invoked any kinematic assumptions while doing so. The *Reissner-Mindlin* plate paradigm accounts for transverse shear strain by handling rotational and translational displacements as 3 independent degrees of freedom. However, as the thickness tends to zero, these shearing effects become negligible and the plate approaches a "pure bending" configuration. The *Kirchhoff-Love* plate model is suitable for thin members for which $\boldsymbol{\zeta} = \mathbf{0}$ is a valid assumption. Consequently, the rotational displacements are simply the negative gradient of the translational displacements.

For isogeometric implementation, we must construct a weak form of (2) consisting of the terms presented in the above strain tensor decomposition. We begin by defining appropriate finite element spaces for the variational formulation. The translational and rotational displacements exist in the spaces

$$\mathcal{S}_w = \mathcal{V}_w := \{w \in \mathcal{H}^1(\Omega) \ : \ w|_{\partial\Omega} = 0\} \quad \text{and} \quad \mathcal{S}_\theta = \mathcal{V}_\theta := \{\boldsymbol{\theta} \in (\mathcal{H}^1(\Omega))^2 \ : \ \boldsymbol{\theta} \times \mathbf{n}|_{\partial\Omega} = \mathbf{0}\}$$

respectively. The *test* and *trial* spaces are then defined by

$$X = \begin{cases} \mathcal{S}_w, & \text{Kirchhoff-Love Plate} \\ \mathcal{S}_w \times \mathcal{S}_\theta, & \text{Reissner-Mindlin Plate} \end{cases} \quad \text{and} \quad Y = \begin{cases} \mathcal{V}_w, & \text{Kirchhoff-Love Plate} \\ \mathcal{V}_w \times \mathcal{V}_\theta, & \text{Reissner-Mindlin Plate} \end{cases}$$

for the mixed variables in the above space

$$\mathbf{u} = \begin{cases} w, & \text{Kirchhoff-Love Plate} \\ (w, \boldsymbol{\theta}), & \text{Reissner-Mindlin Plate} \end{cases} \quad \text{and} \quad \mathbf{v} = \begin{cases} v, & \text{Kirchhoff-Love Plate} \\ (v, \boldsymbol{\eta}), & \text{Reissner-Mindlin Plate} \end{cases}$$

We can then discretize the above spaces and the corresponding mixed variables as

$$\mathcal{S}_w^h := \{w^h \in \mathcal{S}_w \ : \ w^h = \sum_{\mathrm{v}}^{N_\mathrm{v}} u_\mathrm{v} N_\mathrm{v}(\boldsymbol{\xi})\} \quad \text{and} \quad \mathcal{S}_\theta^h := \{\boldsymbol{\theta}^h \in \mathcal{S}_\theta \ : \ \boldsymbol{\theta}^h = \sum_{\mathrm{e}}^{N_\mathrm{e}} \theta_\mathrm{e} \mathbf{M}_\mathrm{e}(\boldsymbol{\xi})\} \tag{5}$$

where N_v and $\mathbf{M}_e$ are isogeometric basis functions for the translational and rotational displacement fields, respectively. We will further specify these functions in what follows. Figure 2 displays representative basis functions for the translational and rotational displacement fields displayed over the parametric domain. The corresponding discrete test and trial spaces X^h and Y^h are defined as X and Y above.

We are now ready to define the constituent weak forms present in the variational formulation. These are arrived at by performing appropriate contractions of the strain tensors (4) with their corresponding constitutive relationships and a virtual displacement. The corresponding bending bilinear form is:

$$\boxed{b_{\text{bending}}(\mathbf{u}, \mathbf{v}) = \int_\Omega C^{\alpha\beta\lambda\mu} \chi_{\alpha\beta}(\boldsymbol{\theta}) \chi_{\lambda\mu}(\boldsymbol{\eta}) \ d\Omega} \tag{6}$$

and the corresponding shear bilinear form is:

$$\boxed{b_{\text{shear}}(\mathbf{u}, \mathbf{v}) = \int_\Omega D^{\alpha\lambda} \zeta_\alpha(w, \boldsymbol{\theta}) \zeta_\lambda(v, \boldsymbol{\eta}) \ d\Omega} \tag{7}$$

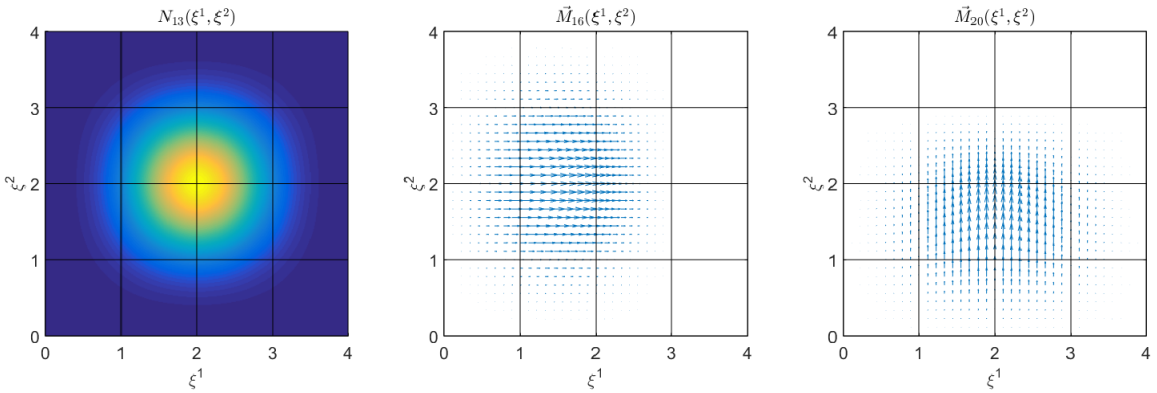

Figure 2: From left to right: A representative scalar (vertex) basis function for translational displacements of polynomial order 3. A corresponding $\boldsymbol{\theta}_1$ vector (edge) basis function for rotational displacements about $\mathbf{a}^2$. A corresponding $\boldsymbol{\theta}_2$ vector (edge) basis function for rotational displacements about $\mathbf{a}^1$.

The virtual work is given by

$$\boxed{F(\mathbf{v}) = t \int_\Omega F v \; d\Omega} \tag{8}$$

where $F = F_3$ for notational convenience. We concern ourselves only with plates subject to transverse loading, so membrane effects (and in-plane displacements) may be neglected. With the above specification of test and trial spaces, and definition of the bilinear forms for bending and shear, isogeometric implementation amounts to solving the following weak problem:

Find $\mathbf{u}^h \in X^h$ *such that*

$$a(\mathbf{u}^h, \mathbf{v}^h) = F(\mathbf{v}^h) \tag{9}$$

for all $\mathbf{v}^h \in Y^h$ *where*

$$a(\mathbf{u}^h, \mathbf{v}^h) = \begin{cases} \dfrac{t^3}{12} b_{\text{bending}}(\nabla w^h, \nabla v^h), & \text{Kirchhoff-Love Plate} \\ \dfrac{t^3}{12} b_{\text{bending}}(\mathbf{u}^h, \mathbf{v}^h) + t b_{\text{shear}}(\mathbf{u}^h, \mathbf{v}^h), & \text{Reissner-Mindlin Plate} \end{cases}$$

and

$$F(\mathbf{v}^h) = \int_\Omega t F v^h \; d\Omega$$

Since (9) will be implemented and subsequently solved through a multigrid method, we must ensure that no issues arise from intergrid transfer e.g., coarsening or refining the mesh. The Kirchhoff-Love equation is fully capable of implementation in a multigrid setting, since only a second derivative term appears in the weak form, provided the NURBS basis is at least C^1-continuous. However, this is not the case for the weak form for the Reissner-Mindlin equation above. In particular, this equation suffers from *locking*, a numerical artifact which arises as a consequence of the "plate" assumption used in the derivation of the model.

This phenomenon can be understood by observing the asymptotic behavior of (9) as the thickness vanishes. This is accomplished by recasting the equation in the form

$$b_{\text{bending}}(\mathbf{u}^h, \mathbf{v}^h) + t^{-2} b_{\text{shear}}(\mathbf{u}^h, \mathbf{v}^h) = \int_\Omega g v \; d\Omega \tag{10}$$

where g is a thickness-scaled loading. It can be shown that as thickness tends to zero, the weak problem (9) reduces to the aforementioned "pure bending" problem

$$b_{\text{bending}}(\mathbf{u}^h, \mathbf{v}^h) = \int_\Omega g v \; d\Omega$$

Conceptually, this illustrates the fact that transverse shear strain, ζ, is negligible for thin members. However, this is the dominant term in the asymptotic limit of (10) above. Therefore, we must have that $\boldsymbol{\zeta} \to \mathbf{0}$ at least quadratically in t as $t \to 0$, which implies that

$$\nabla w \approx -\boldsymbol{\theta} \tag{11}$$

for $t \ll 1$. However for standard isogeometric finite element spaces, this condition must be weakened for compatibility with the basis. For example, consider the limiting case where $t = 0$ and assume piecewise continuous linear basis functions are used for both translational and rotational displacements. Note that piecewise continuous linear basis functions become piecewise constants after differentiation. Moreover, if $\boldsymbol{\theta}$ is to be both continuous and piecewise constant with Dirichlet boundary conditions, (11) implies (erroneously) that $w \equiv 0$ and $\boldsymbol{\theta} \equiv \mathbf{0}$; for $0 < t \ll 1$, this drastically slows convergence rates and generally requires mesh resolution of $h \approx \mathcal{O}(t)$ to overcome locking.

Ultimately, a multigrid method would suffer from locking on the coarse grids in a conventional finite element framework. However, we can construct a *locking-free* implementation by preserving the *plate cohomology* in the choice of basis. This amounts to selecting discrete test and trial spaces which satisfy:

$$\begin{array}{ccc} \mathcal{S}_w & \xrightarrow{\vec{\nabla}} & \mathcal{S}_\theta \\ \downarrow \Pi_w & & \downarrow \Pi_\theta \\ \mathcal{S}_w^h & \xrightarrow{\vec{\nabla}} & \mathcal{S}_\theta^h \end{array} \tag{12}$$

where Π_w and Π_θ are so-called commuting projection operators. Provided such a commuting diagram holds, we have that for any $w^h \in \mathcal{S}_w^h$, there exists a $\theta^h \in \mathcal{S}_\theta^h$ such that the shear constraint $\boldsymbol{\nabla} w^h = -\boldsymbol{\theta}^h$ is satisfied pointwise. We are able to exactly preserve the plate cohomology using the emerging framework of isogeometric discrete differential forms [2]. Within this framework, N_v and $\mathbf{M}_\mathrm{e}$ can be considered as smooth generalizations of the Nédélec elements which exist on the vertices and edges of the mesh, respectively, as displayed by Figure 2.

6 Iterative Schwarz Methods for Overlapping Subdomains

The locking-free Reissner-Mindlin plate paradigm presented above permits the use of multigrid methods for iterative solution, since the prior concern of coarse-grid locking is no longer an issue. However, the nature of the Reissner-Mindlin plate system requires a smoother which respects the coupling between the rotational and translational degrees of freedom in the zero thickness limit. Particularly, we consider the generalization of the Jacobi and Gauss-Seidel smoothers known as Schwarz methods.

Schwarz methods are divided into two schemes, additive and multiplicative. The former is analogous to Jacobi, where the solution is updated only after a complete domain smoothing while the latter is comparable to Gauss-Seidel, where the solution is updated after each smoothing step [5]. The difference between the methods arises in the definition of the entities which are smoothed. Particularly, while Jacobi and Gauss-Seidel smooth nodal quantities, Schwarz methods are applied to pre-defined subdomains; in the case where the subdomains are the individual degrees of freedom, the Schwarz methods coincide with Jacobi and Gauss-Seidel.

For the purpose of the Reissner-Mindlin plate model, we select subdomains with the relationship between translational and rotational degrees of freedom in mind so the smoothing process permits communication between the various displacements. In particular, we specify the subdomains to be the set of functions contained in the support of the vertex basis function i.e., $\Omega_\mathrm{v} = \mathrm{supp}(N_\mathrm{v})$, as shown in Figure 3. This specification ensures that we have a commuting diagram like (12) for each subdomain. This also illuminates the interpretation of Schwarz smoothing solving a series of coupled small-plate problems, where each subdomain is considered to be a small Reissner-Mindlin plate with Dirichlet boundary data specified by translational and rotational displacements of neighboring plate elements. Therefore we consider the *weak subdomain plate problem* posed over the subdomain spaces defined by

$$\mathcal{S}_{w_\mathrm{v}}^h = \mathcal{V}_{w_\mathrm{v}}^h := \{w^h \in \mathcal{S}_w^h \ : \ \mathrm{supp}(w^h) \subset \Omega_\mathrm{v}\} \quad \text{and} \quad \mathcal{S}_{\theta_\mathrm{v}}^h = \mathcal{V}_{\theta_\mathrm{v}}^h := \{\boldsymbol{\theta}^h \in \mathcal{S}_\theta^h \ : \ \mathrm{supp}(\boldsymbol{\theta}^h) \subset \Omega_\mathrm{v}\} \tag{13}$$

and furthermore the subdomain test and trial spaces defined by

$$X_v^h := \begin{cases} \mathcal{S}^h_{w_\mathrm{v}}, & \text{Kirchhoff-Love Plate} \\ \mathcal{S}^h_{w_\mathrm{v}} \times \mathcal{S}^h_{\theta_\mathrm{v}}, & \text{Reissner-Mindlin Plate} \end{cases} \quad \text{and} \quad Y_v^h := \begin{cases} \mathcal{V}^h_{w_\mathrm{v}}, & \text{Kirchhoff-Love Plate} \\ \mathcal{V}^h_{w_\mathrm{v}} \times \mathcal{V}^h_{\theta_\mathrm{v}}, & \text{Reissner-Mindlin Plate} \end{cases}$$

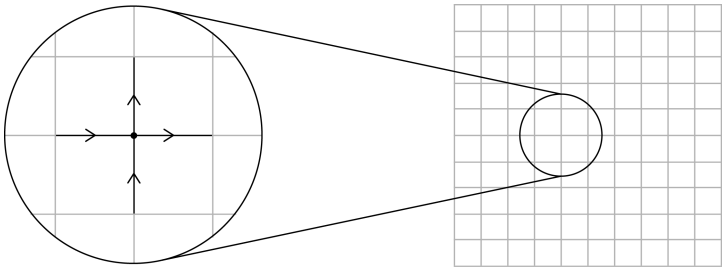

Figure 3: A representative subdomain defined by the support of the vertex basis function and containing the adjacent edge basis functions.

After defining the overlapping subdomains, we are ready to present the Schwarz methods used for iterative smoothing of the numerical solution. Through the subdomain definition, we are able to construct restriction and prolongation operators that isolate and combine the corresponding subdomain stiffness matrices.

Consider the domain for a fixed level l of the multigrid method such that $\Omega^l = \cup_\mathrm{v} \Omega^l_\mathrm{v}$, where $\Omega^l_\mathrm{v} = \Omega_\mathrm{v}$. We define restriction and prolongation operators via $R_\mathrm{v} : \Omega^l \to \Omega^l_\mathrm{v}$ and $R^T_\mathrm{v} : \Omega^l_\mathrm{v} \to \Omega^l$. The n^{th} iteration of the Schwarz method begins by first computing the residual $\mathbf{r}^n = \mathbf{f} - A\mathbf{u}^n$. The additive Schwarz method is then defined via

$$\mathbf{u}^{n+1} = \mathbf{u}^n + \eta \left(\sum_{\mathrm{v}=1}^{N} R^T_\mathrm{v} (R_\mathrm{v} A R^T_\mathrm{v})^{-1} R_\mathrm{v} \right) \mathbf{r}^n$$

where $\eta \in (0, 1]$ is the *scaling factor*. This factor is introduced because additive Schwarz does not preserve the partition of unity hence will not converge, as introduced in [7]. The multiplicative Schwarz method for N subdomains is defined as

$$\mathbf{u}^{n+\frac{i}{N}} = \mathbf{u}^{n+\frac{i-1}{N}} + R^T_\mathrm{v} (R_\mathrm{v} A R^T_\mathrm{v})^{-1} R_\mathrm{v} \mathbf{r}^{n+\frac{i-1}{N}}$$

7 Numerical Tests

We now present a series of numerical tests illustrating the effectiveness of our proposed multigrid framework. The first test is a weakly clamped rectangular Kirchhoff-Love plate with uniform downward loading. The exact solution to this problem is known and used as an assessment of convergence. Figure 4 contains a table displaying the number of V-cycles required to reduce the error by 10^6, along with the corresponding average convergence factor during this process, for various numbers of degrees of freedom. For each V-cycle, one pre and post smoothing step is employed using the multiplicative Schwarz smoother. From the figure, we observe that the number of iterations required for error reduction is independent of the number of levels. Figure 5 demonstrates the convergence of the numerical solution with mesh refinement if a full multigrid algorithm is employed for system solution. From the figure, we observe the convergence is optimal with respect to mesh refinement. That is, the error decays like N^{-2}, where N is the number of degrees of freedom.

Our second test is a weakly-clamped parallelogram Kirchhoff-Love plate with uniform downward loading. As opposed to the first test, the exact solution to this test exhibits singularities in the obtuse corners which inhibit convergence. Figure 6 contains a table displaying the number of V-cycles required to reduce the error by 10^6, along with the corresponding average convergence factor during this process, for various numbers of degrees of freedom. The V-cycles for this problem are identical to the rectangular plate case. From the figure, we observe that the number of iterations required for error reduction is asymptotically independent of the number of levels, though the number of iterations required for convergence for this problem is larger than the number required for the first problem. This detoriation is a consequence of the singularities present in the exact solution.

DOFs	V-cycles	Convergence Factor
16	9	0.211
25	10	0.241
49	9	0.203
121	9	0.213
361	10	0.229
1225	10	0.226

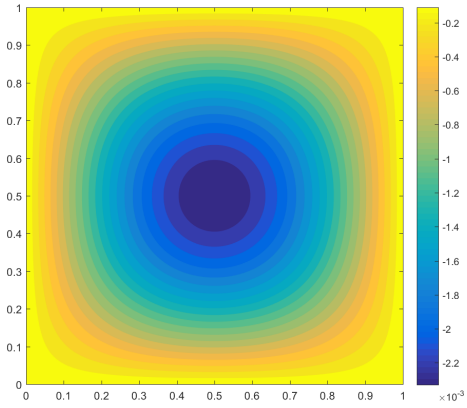

Figure 4: Convergence behavior and displacement plot for the rectangular Kirchhoff-Love plate system using a $V(1,1)$ scheme.

DOFs	Error	Convergence Rate
16	2.879e-05	-
25	3.698e-06	4.5985
49	3.863e-07	3.3568
121	6.404e-08	1.988
361	3.528e-09	2.6519
1225	4.781e-10	1.6358

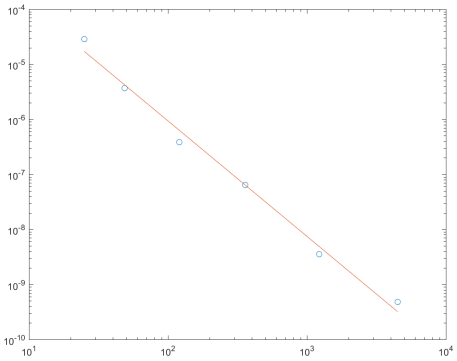

Figure 5: Convergence rates and plot of $\|\mathbf{e}\|_{L^2}$ at various levels of refinement for the rectangular Kirchhoff-Love plate using FMG(1,1,1) scheme.

DOFs	V-cycles	Convergence Factor
16	6	0.092
25	13	0.341
49	39	0.699
121	65	0.808
361	82	0.845
1225	86	0.851

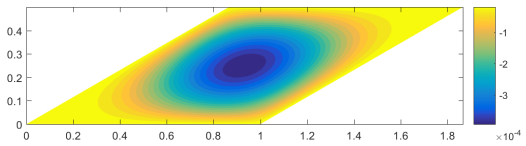

Figure 6: Convergence behavior and displacement plot for the parallelogram Kirchhoff-Love plate system using a $V(1,1)$ scheme.

Next, results for the weakly clamped, rectangular Reissner-Mindlin plate with uniform loading are presented. Table 1 shows the number of V-cycles required to reduce the norm of the residual by 10^6, along with the average convergence factor during this process, for various levels of refinement. Similarly to the Kirchhoff-Love plate, one pre and post smoothing step is employed using the multiplicative Schwarz smoother, for each V-cycle. From the figure, we observe that the number of iterations required for error reduction is independent of the number of levels. Perhaps more importantly, the convergence rate is independent of the plate thickness. This is the first time this has been observed for a Reissner-Mindlin plate discretization in its primal form. This observation has considerable implications in engineering practice. The ability to develop robust, efficient, and easy to implement multigrid methods for beams, plates, and shells

has the potential to dramatically reduce the cost associated with structural mechanics simulations. This is made further evident when coupled with the enhanced robustness and accuracy of isogeometric analysis, as compared to classical finite element analysis.

Table 1: Convergence behavior of the rectangular Reissner-Mindlin plate for at various thicknesses with the multiplicative Schwarz smoother. The "V-cycles" column presents the number of V(1,1)-cycles required to reduce the residual by 10^6. The "Convergence Factor" column is the average convergence factor through this process.

DOFs	$t = 0.05$		$t = 0.01$		$t = 0.001$		$t = 0.0001$	
	V-cycles	Convergence Factor	V-cycles	Convergence Factor	V-cycles	Convergence Factor	V-cycles	Convergence Factor
65	22	0.528	23	0.541	19	0.479	16	0.416
133	24	0.562	25	0.572	24	0.560	20	0.498
341	19	0.480	20	0.498	19	0.482	19	0.481
1045	17	0.436	18	0.458	18	0.458	18	0.459
3605	12	0.313	15	0.390	16	0.419	16	0.420
13333	12	0.310	14	0.362	15	0.392	15	0.396

The additive Schwarz method lends itself to efficient parallel implementation, as opposed to the multiplicative Schwarz method. As a final test, we examined the effectiveness of the additive Schwarz method as a smoother for the weakly clamped rectangular Reissner-Mindlin plate. Figure 7 contains a table displaying the number of V-cycles required to reduce the error by 10^6, along with the corresponding average convergence factor during this process, for various numbers of degrees of freedom. From the figure, we observe that the number of iterations required for error reduction is independent of the number of levels though the convergence factor is higher than that associated with a multiplicative Schwarz smoother. This deterioration in convergence is offset by the lower computational cost of the additive Schwarz method, as well as its capability for parallel implementation.

DOFs	V-cycles	Smoothing Factor	Convergence Factor
65	35	0.4	0.671
133	40	0.4	0.705
341	62	0.4	0.800
1045	60	0.4	0.793
3605	51	0.4	0.762
13333	49	0.3*	0.754

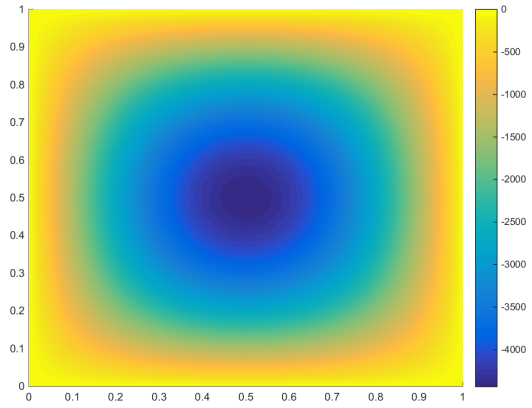

Figure 7: Convergence behavior for a $V(1,1)$-cycle and displacement plot for the ($t = 0.0001$) rectangular Reissner-Mindlin plate system of 13333 DOFs solved using full multigrid with the additive Schwarz smoother. *A smoothing factor of $\eta = 0.3$ was required for the solution to converge on the finest mesh.

Numerical tests were also run for problems with complex geometry and various loadings. Similar results were achieved in these cases, further demonstrating the robustness of the proposed framework. The results of these tests are not shown for brevity.

8 Conclusions and Future Work

In this paper, we presented a locking-free isogeometric approach to the numerical solution of the classical Reissner-Mindlin and Kirchhoff-Love plate equations. The isogeometric paradigm automatically provides the necessary continuity for a weak implementation of the Kirchhoff-Love plate, while the algebraic structure of isogeometric discrete differential forms yields a robust and accurate method for the Reissner-Mindlin plate, independent of plate thickness. Our new approach permits linear system solution through a geometric multigrid method. This is in contrast with classical approaches, which require the use of expensive direct solvers. Our multigrid methods leverage the use of additive and multiplicative Schwarz smoothers with overlapping subdomains. This illuminates the interpretation of the overall problem as a system of coupled plates with Dirichlet boundary data specified by neighboring subdomains. Illustrative numerical tests were provided that demonstrate our method is robust and converges with rates independent of the plate thickness and mesh size.

In future work, we will extend the presented method to classical and shear-deformable shells. We anticipate that the present method may be easily extended to this setting, though we expect modifications will be required to address the problem of membrane locking. Thereafter, we will extend our framework to complex structures consisting of multiple beams, plates, and shells (e.g., an airplane wing). Application of our framework to such complex structures will require the use of parallel implementation to to alleviate simulation cost and to simultaneously deal with increased memory requirements. Finally, we anticipate that our framework may be easily extended to incompressible fluid flow problems by exploiting the existence of a Stokes cohomology [6, 7].

References

[1] D. N. Arnold, R. S. Falk, and R. Winther. Preconditioning discrete approximations of the Reissner-Mindlin plate model. *RAIRO-Modélisation mathématique et analyse numérique*, 31(4):517–557, 1997.

[2] L. Beirão da Veiga, A. Buffa, C. Lovadina, M. Martinelli, and G. Sangalli. An isogeometric method for the Reissner-Mindlin plate bending problem. *Computer Methods in Applied Mechanics and Engineering*, 209:45–53, February 2012.

[3] D. Chapelle and K. J. Bathe. *The Finite Element Analysis of Shells - Fundamentals*. Computational Fluid and Solid Mechanics. Springer, 2003.

[4] J. A. Cottrell, T. J. R. Hughes, and Y. Bazilevs. *Isogeometric Analysis: Toward Integration of CAD and FEA*. Wiley Publishing, 1st edition, 2009.

[5] V. Dolean. *An Introduction to Domain Decomposition Methods : Algorithms, Theory, and Parallel Implementation*. Society for Industrial and Applied Mathematics, Philadelphia, 2015.

[6] J. A. Evans and T. J. R. Hughes. Isogeometric divergence-conforming B-splines for the Darcy–Stokes–Brinkman equations. *Mathematical Models and Methods in Applied Sciences*, 23(04):671–741, 2013.

[7] G. Kanschat and Y. Mao. Multigrid methods for H(div)-conforming discontinuous Galerkin methods for the Stokes equations. *ArXiv e-prints*, January 2015.

[8] L. Piegl and W. Tiller. *The NURBS Book*. Springer Science & Business Media, 2012.